Automatic Detection of Ultrasound Contrast Microbubble Shell Rupture

A.Y. Ammi, L. Bridal
Laboratoire d'Imagerie Paramétrique
UMR 7623 CNRS; Université Paris6
Paris, France
bridal@lip.bhdc.jussieu.fr

J. Mamou, G.I. Wang, W.D. O'Brien, Jr
Bioacoustics Research Laboratory
University of Illinois
Urbana-Champaign, IL, USA
wdo@uiuc.edu

***Abstract*—Characterizing occurrence of ultrasound contrast agent (UCA) microbubble destruction is important for development of functional and therapeutic applications. Previously [1], it was demonstrated that post-excitation acoustic emissions detected with passive cavitation detection (PCD) result from inertial cavitation (IC) of UCA after shell rupture. That work relied on time-consuming visual inspection of PCD data to identify IC signals and characterized only minimum rarefactional pressure thresholds for rupture of a single Optison™ microbubble in the sampled population. This work introduces an algorithm for automatic detection of IC signals. The algorithm was applied to the 71424 waveforms in the PCD data set. At each incident frequency (0.9, 2.8 or 4.6 MHz) and pulse duration (3, 5 or 7 cycles) combination, ruptured microbubble occurrence with incident peak rarefactional pressure (PRP) was well described by a logistic regression curve with an inflection point near 50% occurrence and a plateau at 100%. With a 5-cycle pulse duration at 0.9, 2.8 and 4.6 MHz the incident PRPs leading to 5% microbubble rupture were 0.66, 0.83 and 1.1 MPa; and 1.1, 1.6 and 2.5 MPa for 50%. This automatic algorithm combined with the PCD approach provides a practical tool for the characterization of UCA destruction occurrence across a significant range of incident PRPs.**

Keywords- ultrasound contrast agent; destruction; microbubbles; cavitation

I. INTRODUCTION

Microbubble (MB) destruction plays a key role in many ultrasonic contrast techniques used or under evaluation in the clinic. By destroying contrast MBs with a high-amplitude acoustic pulse and then observing the refill of MBs at lower acoustic pressure levels, information on the kinetics of flow can be obtained [2]. Imaging of strongly scattering, short-lived free bubbles with a unique acoustic signature produced by the acoustic rupture of contrast MB shells has also been proposed [3]. Several researchers are exploring MBs as drug delivery vehicles, which can be concentrated in a specific area [4] and then ruptured with acoustic pulses to assure controlled and localized treatment.

Experimental data are needed to better understand and quantify UCA destruction thresholds. Several experimental approaches have been used to respond to this need. Direct optical observation [5] is currently the reference for measuring UCA destruction thresholds. However, the expensive equipment necessary for its application limits the technique's accessibility, it is not transferable to *in vivo* studies of optically opaque human organs and optical isolation of one MB at a time generally limits the number of sampled bubbles studied. Acoustic attenuation has also been used to evaluate UCA destruction [6]. Onset of destruction, however, remains elusive with this approach which provides rather a measurement of the peak rarefactional pressure (PRP) causing total destruction of UCAs in a suspension. Active cavitation detection (ACD) has been used to estimate UCA collapse thresholds, where the receiver interrogates the region of interest with a low-pressure pulse amplitude in order to assess the potential cavitation effects from another ultrasound exposure of that same region [6, 7]. The passive cavitation detector (PCD) technique is related to the ACD approach but uses a passive receiver to listen for acoustic emissions from MBs excited by another source [1, 8, 9]. Optison™ PRP thresholds from PCD measurements at similar incident frequencies but with different criteria to identify destruction are summarized in Table I.

TABLE I. OPTISON™ DESTRUCTION THRESHOLDS REPORTED FOR PCD

Criteria	Frequency (MHz)	Pulse Duration	PRP (MPa)
Broadband noise emission > 1σ of noise[a]	1.1	~ms	0.2
Increased broadband noise and > 5 % voltage spikes above noise[b]	1.1	~µs	0.13
Detection of one post-excitation IC signal[c]	0.9	~µs	0.29
Broadband noise emission > 1σ of noise[a]	3.3	~ms	1.6
Increased broadband noise and > 5 % voltage spikes above noise[b]	3.5	~µs	0.48
Detection of one post-excitation IC signal[c]	2.8	~µs	0.71

a. Ref. [8], b. Ref. [9], *c.* Ref. [1], σ, standard deviation; IC, inertial cavitation

The summary in Table I reveals that the estimated destruction levels for a UCA vary depending on the criteria applied for destruction detection. Furthermore, measurements of destruction thresholds are available for only a few tested incident PRPs, pulse durations (PD) or frequencies.

This work presents an automated approach for the detection of inertial cavitation (IC) signals in PCD data that provides the basis for an objective technique characterizing MB destruction occurrence across a large range of PRPs.

II. Materials and Methods

A. Contrast agent

Experiments were conducted using Optison™ (Mallinckrodt and Molecular Biosystems, San Diego, CA), an FDA-approved UCA. Optison™ MBs have an albumin shell, approximately 15-nm thick, encapsulating perflutren C_3F_8 gas. The solution in the manufacturer's vial has a concentration between 5 and 8 x 10^8 MBs/mL. Approximately 93% of the MB diameters are less than 10 µm, with a maximum diameter of 32 µm and a mean diameter in the range of 2-4.5 µm.

B. Passive Cavitation Detector

The PCD setup is described in detail elsewhere [1]. Briefly, it consists of a passive receiver (13-MHz center frequency) aligned at 70° and confocal to a transmitter (0.9, 2.8 or 4.6 MHz center frequency). The transducers were immersed in gently stirred water containing a very dilute concentration of UCAs. The transmit transducer was excited with a sinusoidal pulse (3, 5 or 7 cycles) having a PRP at the transducer focus between 0.07 and 5.4 MPa. The signal received with the passive receiver was amplified, digitized (12-bit, 200 MHz) and saved to a personal computer. For each PD, frequency and PRP setting, the above data acquisition sequence was repeated 128 times (every 100 ms). The UCA solution was diluted relative to the confocal detection volume such that, on average, at most one UCA MB should be interrogated with each incident pulse.

In previous work [1], we established that post-excitation signals (Fig. 1) detected with the PCD were linked to IC and rebound events. Thus, the detection of these signals could be used to evaluate UCA rupture.

C. Automatic IC detection

For a given frequency and PD, each of the 128 acquired waveforms acquired with the PCD system was truncated to keep a 4000-sample segment (20-µs duration) centered at the time-of-flight (TOF) to the confocal zone of the transmit and receive transducers. The signal at the center of this segment is the bubble response during acoustic excitation (principal response). Prior to the principal response during bubble excitation only noise is detected by the passive receiver. Any IC acoustic emissions related to MB destruction should occur in the record length of this segment, recorded after MB excitation.

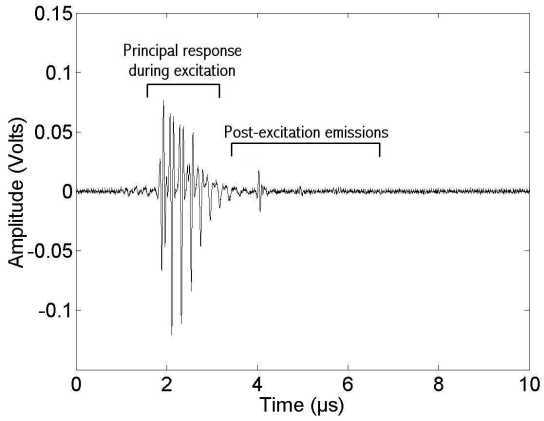

Figure 1. Central segment of a signal received with the PCD.

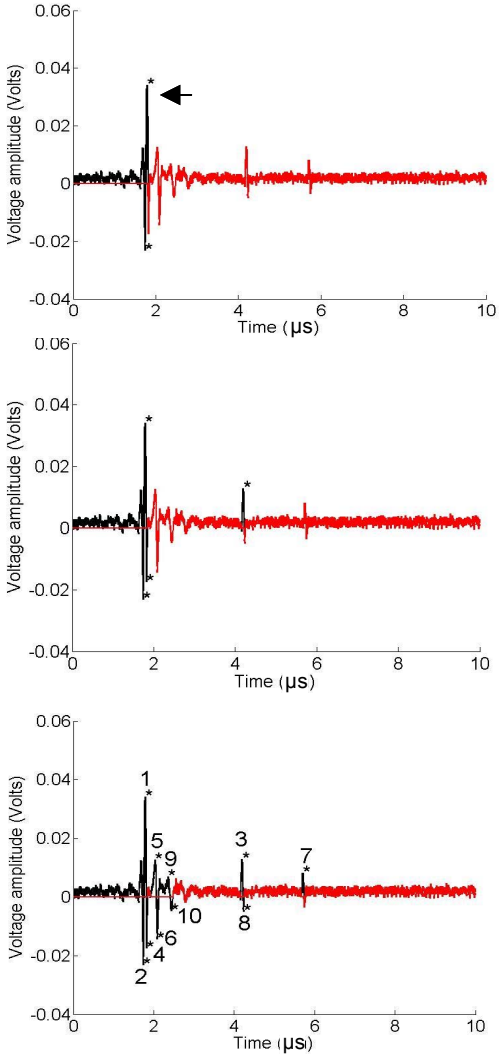

Figure 2. Central 10-µs of a PCD signal illustrating peak detection algorithm. a) First peak pair (*) and principal peak (arrow) b) Second peak pair detected (*) c) All detected peaks numbered in order of detection. Dark black segments of signal at each step have been eliminated from further peak detection.

Work supported by cooperative project for biomedical engineering: University of Illinois at Urbana-Champaign, USA and the Centre National de la Recherche Scientifique, France; and by NIH R37EB002641.

The DC component of the signal is removed by subtracting the mean voltage value. The maximum absolute voltage amplitude in the first 100 samples of the segment is the maximum noise signal amplitude, V_{max_noise}. Next the maximum positive peak and the maximum negative peak are detected (Fig. 2). Their voltage amplitudes and temporal positions are recorded (Table II). Of these two peaks, the one occurring at a later time is defined to be the *principal peak*. Because the principal peak is always observed during the principal response of the acoustically excited MB, the algorithm's search for an IC event only considered the segment of the signal following the *principal peak*. All points between the *principal peak* and the nearest, following zero-crossing were also excluded from further peak detection. The positive and negative peaks with the next greatest absolute amplitudes following those of the first two detected peaks are detected. Their temporal positions and amplitudes are recorded (Table II). All points in the half-cycle between the two zero-crossings on either side of each of these detected peaks are exempted from further peak detection. The automatic peak detection algorithm continues detecting peak pairs in the order of decreasing absolute amplitude and exempting points within the zone bounded by zero-crossings on either side of the peaks from further search until one of the following criteria is satisfied:

- A peak is detected with an absolute magnitude < $|V_{max\_noise}|$,
- A peak is detected at the very edge of the record length or at the very edge of a segment of the record length that has previously been excluded from the search segment.

TABLE II. DETECTED PEAKS

Positive Peaks			Negative Peaks		
#	*Delay (μs)*	*Amplitude |V|*	#	*Delay (μs)*	*Amplitude |V|*
1	1.79	0.0342	2	1.73	0.0232
3	4.19	0.0129	4	1.82	0.0173
5	2.03	0.0127	6	2.08	0.0144
7	5.70	0.0080	8	4.23	0.0048
9	2.35	0.0068	10	2.43	0.0046

Once all peaks have been detected peak amplitudes and temporal positions were compared as illustrated in Table III for the positive peaks.

TABLE III. ILLUSTRATION OF PEAK COMPARISON

Delay (μs)	**Amp. |V|**	**Peak #**	**Peaks compared**	**Δt (μs)**	**Δ amplitude (V)**
1.79	0.0342	1	5 - 1	0.24	-0.215
2.03	0.0127	5	9 - 5	0.32	-0.0059
2.35	0.0068	9	3 – 9	**1.84**[a]	**0.0061**[b]
4.19	0.0129	3			

a. The time between consecutive peaks, Δt, >> than the period of the excitation pulse (excitation = 2.8 MHz, period ~ 0.36 μs) b. The amplitude of peaks increases with increasing time-of-flight.

Each segment was then classified into one of four groups:

- **MB detected but no destruction.** At least three peaks were detected. These peaks decreased in amplitude as a function of the detection time, and the temporal spacing between consecutive peaks of the same sign was consistent with time between periods of the excitation pulse.
- **MB detected with destruction.** At least three peaks were detected. Peaks did not decrease systematically in amplitude as a function of the detection time or the temporal spacing between at least one pair of consecutive peaks of the same sign was not consistent with the time between periods of the excitation pulse.
- **No MB detected.** No peak was detected.
- **Requiring visual inspection to classify.** Only one or two peaks were detected.

III. RESULTS

For each frequency, PD and incident PRP combination, the percent occurrence of MB destruction was estimated the results of the IC detection for the 128 waveforms according to:

$$\text{Occurrence} = [N_1/(N_1+N_0)]\times 100, \quad (1)$$

where N_1 is the number of signals classified as MBs detected with destruction and N_0 is the number of signals classified as detected MBs without destruction. For each set of parameters, the results were plotted as a function of PRP (Fig. 4). MB rupture occurrence increased progressively from the minimum incident PRP at which IC was first detected through an inflection point near 50% destruction towards a plateau of 100 % destruction. The range of PRP studied for an incident pulse at 0.9 MHz did not include PRPs producing 100% destruction. The larger ranges considered at incident frequencies of 2.8 and 4.6 MHz present results from 0 to nearly 100% destruction in all but one case (3-cycle, 4.6-MHz pulse). The data were fit to a logistic regression (solid curve in Fig. 4). Based on the logistic regression statistics fit to the data, the 5% and 50% MB destruction occurrence levels were calculated.

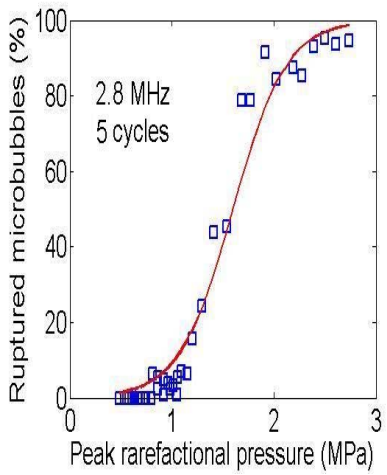

Figure 3. Occurrence of Optison™ MB destruction as a function of the PRP for a 5-cycle, incident pulse at 2.8-MHz center frequency.

IV. Discussion and Conclusion

To enable the automatic detection of peaks indicating IC, an algorithm was developed to detect all peaks of each PCD signal and then to compare their spacing and amplitudes. This automatic process was applied to classify PCD signals as unruptured oscillating MBs or ruptured MBs. Although, near the PRP where the first IC event was observed for each set of insonification parameters, a few signals (from 5 to 8 out of 128) were not able to be classified automatically, and classification was attempted by visual analysis of the signal, the large majority of signals were classified automatically. The time taken for the automatic analysis of a set of 128 signals was on the order of 7 minutes using a Xeon™ CPU 2.66 GHz. This automatic IC-detection ability is central to making the PCD approach a practical tool for examining the stochastic process of MB destruction.

The current work extends previous estimations of the minimum PRP leading to a single MB rupture event to estimate the percent occurrence of MB rupture as a function of PRP. This original approach permitted the study of the evolution of the percentage of ruptured MBs as a function of the incident PRP. The 50% thresholds were on the order of 2 to 3 times higher than the PRPs producing a single rupture event at all frequencies except for the case of 7 cycles at 0.9 MHz. The more detailed threshold information obtained in this study should be useful in selecting the pulse characteristics to apply for imaging (minimized MB destruction) and therapeutic (maximized MB destruction) applications.

References

[1] A. Ammi, R.O. Cleveland, J. Mamou, G.I. Wang, S.L. Bridal, W.D. O'Brien, Jr "Ultrasonic contrast agent shell rupture detected by inertial cavitation and rebound signals," IEEE Trasn Ultrason Ferroelec Freq Cont, vol. 53, pp. 126-136, 2006.

[2] K. Wei, A.R. Jayaweera, S. Firoozan, A. Linka, D.M. Skyba, S. Kaul "Quantification of myocardial blood flow with ultrasound-induced destruction of microbubbles administered as a constant venous infusion," Circulation, vol. 97, pp. 473-483, 1998.

[3] F. Forsberg, W.T. Shi, M.K. Knauer, A.L. Hall, C. Vecchio, R. Bernardi "Real-time excitation-enhanced ultrasound contrast imaging," Ultrason Imaging, vol. 27, pp. 65-74, 2005.

[4] H. Leong-Poi, J Christiansen, P. Heppner, C.W. Lewis, A.L. Klibanov, S. Kaul, J.R. Lindner, "Assessment of endogenous and therapeutic arteriogenesis by contrast ultrasound molecular imaging of integrin expression. Circulation, vol. 111, pp. 3248-3254. 2005.

[5] J.E. Chomas, P.A. Dayton, D. May, J. Allen, A. Kibanov, K Ferrara "Optical observation of contrast agent destruction," Applied Physics Letters, vol. 77, pp. 1056-1058, 2000.

[6] P.P. Chang, W.S. Chen, P.D. Mourad, S.L. Poliachik, L.A. Crum, "Thresholds for inertial caviation in Albunex suspensions under pulsed ultrasound conditions," IEEE Trans Ultrason Ferroelectr Freq Control, vol. 48, pp. 161-170, 2001.

[7] L.A. Crum , R.A. Roy, M.A. Dinno, C.C. Church, R.E. Apfel, C.K. Hollang, S.I. Madanshetty "Acoustic cavitation produced by microsecond pulses of ultrasound: a discussion of some selected results," J Acoust Soc Am, vol. 91, pp. 1113-1119, 1992.

[8] T. Giesecke and K. Hynynen, "Ultrasound-mediated cavitation thresholds of liquid perfluorocarbon droplets in vitro," Ultrasound Med Biol, vol. 29, pp. 1359-1365, 2003.

[9] W.S. Chen, T.J. Matula, A.A. Brayman, L.A. Crum, "A comparison of the fragmentation thresholds and inertial cavitation doses of different ultrasound contrast agents. J Acoust Soc Am, vol. 113, pp. 643-651, 2003.